The orientational order/disorder transition in buckminsterfullerene (C_{60}): an experiment using the NCNR Disk Chopper Spectrometer

Summer School on Methods and Applications of Neutron Spectroscopy
NIST Center for Neutron Research
June 20-24, 2005

Craig Brown, John Copley and Yiming Qiu

Abstract

Time-of-flight neutron spectroscopy will be used to examine the orientational order/disorder transition in buckminsterfullerene. This experiment not only illustrates the important technique known as quasielastic neutron scattering (QENS), but also shows how one can simultaneously study the structure and the phonon density of states of C_{60}. We shall discuss all aspects of the experiment, from sample preparation and the choice of instrumental setup through to data treatment and interpretation of results.

I. Introduction

For the past fifteen years there has been intense research into the structural, electronic, magnetic and chemical properties of the two newest allotropes of carbon, namely Buckminsterfullerene and nanotubes (arguably there are more), and their derivatives. The best-known carbon allotropes are:

3-dimensional (3D) diamond

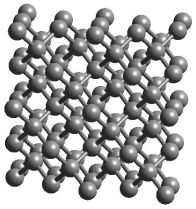

2-dimensional (2D) graphite

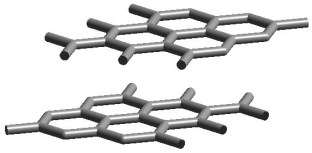

1-dimensional (1D) carbon nanotubes

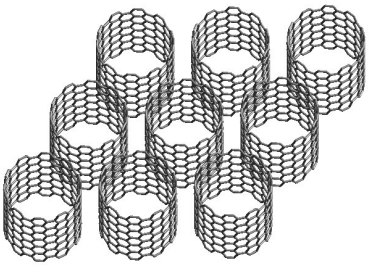

Solid C_{60} composed of 0-dimensional (0D) C_{60} molecules in a cubic lattice.

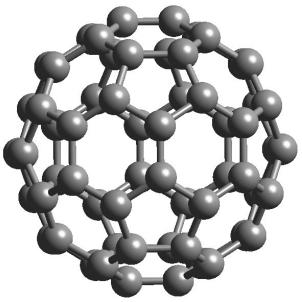

Figure 1. In diamond there is only one characteristic bond length which is ~1.55 Å. In graphite there are two relevant interatomic distances; namely 1.42 Å within the graphite sheets and ~3.4 Å between the sheets, defining the 2D structure. Nanotubes can have four different characteristic distances; carbon-carbon bond distance within each shell (which is almost the same as in graphite), the distance between shells (which is similar to the distance between the graphite layers), the length of the tube (which can reach up to 1mm) and the radius of the tube (which can vary from 10 Å to 100 Å). C_{60} has two characteristic distances; the C-C bond length which is 1.40 Å and 1.45 Å for double and single bonds, respectively

The C_{60} molecule consists of sixty symmetry-equivalent carbon atoms with 12 isolated pentagons and 20 hexagons making the familiar soccer shaped molecule (or a truncated

icosahedron) with point group symmetry, *Ih*. Its electronic properties are determined by the 60 $p\pi$ C orbitals, which are filled by 60 electrons. Crystallization results in the formation of a crystal structure that is face centered cubic (fcc) above 260 K with the molecules packing in a cubic arrangement with the distance between the centers of molecules being about 10 Å. It is possible to describe experimental X-ray powder data using a model consisting of a uniform shell of electron density (radius= 3.55 Å) in place of the C_{60} units within space group Fm3m (a= 14.1569(5) Å at 290 K). However, a better description of X-ray diffraction data is provided by using symmetry adapted spherical harmonic (SASH) functions (essentially derived from linear combinations of spherical harmonic functions, $Y_{lm}(\theta,\phi)$). In the fcc lattice, the scattering density shells occupy the 4a sites of O_h symmetry, necessitating only the SASH functions with values for l= 0, 6, 10 and 12. This analysis results in an excess charge density of ~10% along the <100> and a deficiency of ~16% along the <111> directions. In addition, the Bragg peaks ride on a distinctively humped diffuse background (fig. 2), the origins of which you should be able to guess, by the end of this course.

On cooling through 260 K, a first order structural phase transition occurs, with the reorientational motion of the C_{60} molecules in the crystal becoming slower and now best described as a librational motion. The phase transition is accompanied by a sudden contraction of 0.344(8)% in the cubic lattice constant. Reflections not compatible with fcc symmetry are now present in the powder diffraction patterns, reflecting a long range orientational ordering of the fulleride units and a primitive cubic, $Pa\bar{3}$, space group. The orientations of the four molecules occupying the positions (0,0,0), (½,0,½), (½,½,0) and (0, ½,½) in the new unit cell can be described starting from the so-called "standard orientation", in which the [100] crystallographic axes align with three twofold molecular symmetry axes (perpendicular to hexagon-hexagon fusions) and the [111] crystallographic axes pass through the centres of hexagonal faces. Each of the molecules is then rotated anticlockwise by an angle ϕ about the [111], $[\bar{1}\bar{1}1]$, $[1\bar{1}\bar{1}]$ and $[\bar{1}1\bar{1}]$ axes, respectively (fig.2).

Rietveld refinement of neutron powder diffraction data identified two types of C-C bonds related to short 'double bonds' (1.40 Å) and long 'single bonds' at 1.45 Å. The double bonds, also known as 6:6 bonds, fuse two hexagons together whereas the longer hexagon:pentagon fusions are known as 6:5 bonds. The experimentally determined structure comprises a majority fraction of molecules rotated by ϕ~98^o from the so-called standard orientation, so that optimization of intermolecular interactions occurs with electron-rich double bonds lying over electron-deficient *pentagonal* faces of neighboring molecules. A co-existing minority orientation is only slightly less energetically favorable (by ~11 meV) and is characterized by the alignment of 6:6 bonds parallel to *hexagonal* faces of neighbors with a rotation angle of ϕ~38^o from the standard orientation.

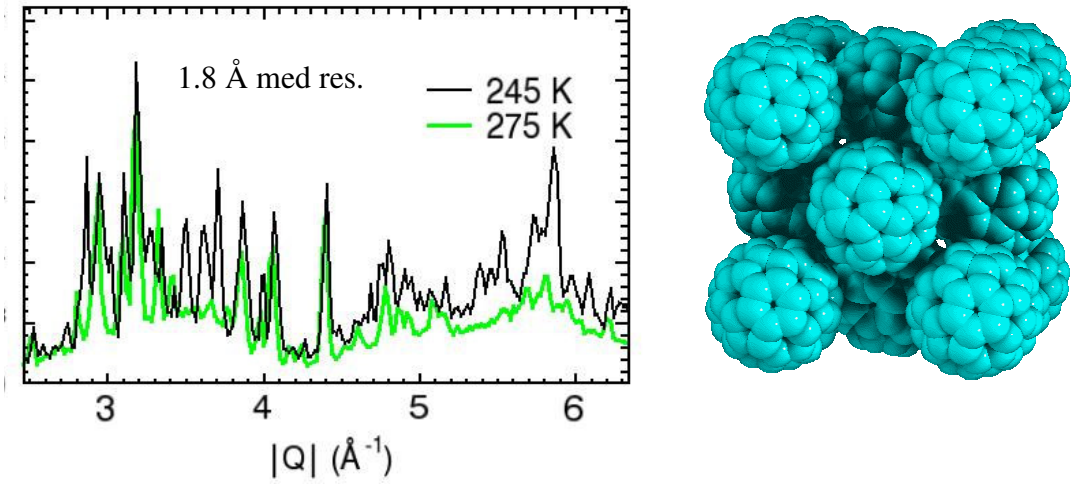

Figure 2. Elastic scattering from C_{60} measured on the DCS at 1.8 Å, in "medium resolution" mode, above and below the 260 K order-disorder phase transition. The counting time was 2 hours. To the right is a view of the unit cell of the simple cubic low temperature phase of C_{60}.

Inelastic neutron scattering (INS) measurements have identified librational peaks at ~2.5 meV at 100 K (and we will perform similar measurements), while motional narrowing of lines in ^{13}C NMR spectra was also observed. The dynamics in the primitive cubic phase were initially attributed to jumps between the almost degenerate orientations, via 60° hops about <111> axes. This however gives rise to a uniaxial reorientation where only three of the 60 equivalent orientations are visited. Alternatively the reorientation can be thought of as occurring via ~36° rotations about <110> axes. Two successive hops about the same axis are unfavorable as this would place a pentagon perpendicular to the [111] direction. The resultant pseudo-random sequence of uniaxial reorientations has a quasi-isotropic nature and all 60 equivalent orientations can be accessed. On the assumption that this is the dominant reorientational mechanism, a cosine potential can be used to approximate the uniaxial rotational potential.

On cooling from 260 K to ~90 K, the fraction of molecules in the majority 98° orientation increases from roughly 60% to ~83.5%, whereas below 90 K the fraction of molecules in the 98° orientation remains constant at ~83.5% because the molecules now have insufficient energy to overcome the potential barrier separating the two orientations. A cusp in the rate of change of lattice constant with temperature is observable at the same temperature, as shown in Fig.3. The dynamics of the C_{60} molecules are extremely limited performing only small amplitude librational motion. Heat capacity measurements have identified this as a subtle transition in comparison to the high temperature first-order transition. The onset of orientational glass behavior is attributed to molecular orientational disorder which is frozen in, as a consequence of the long relaxation time of the molecular reorientations.

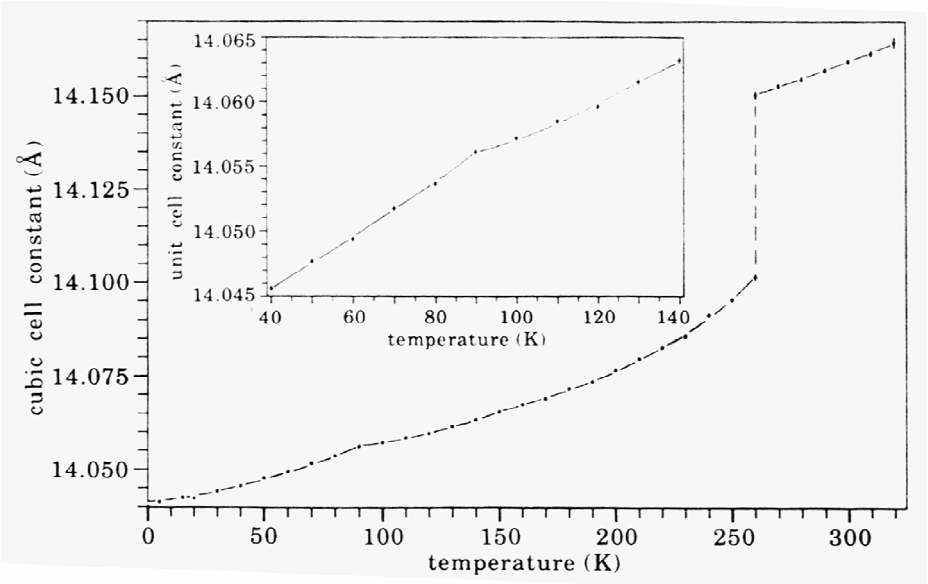

Figure 3. Evolution of the cubic lattice constant for C_{60} as a function of temperature. A first order phase transition occurs at 260 K that is accompanied by a discontinuous jump in the lattice parameter. A cusp is discernible at 90 K, as highlighted in the inset.

The neutron has several properties that enable scattering experiments to measure properties of materials that other techniques can measure with much less precision or not at all. Neutrons with wavelengths on the order of interatomic spacings also possess energies on the same order as those characteristic of phonons and intermolecular interactions; for example, a 1.8 Å neutron has an energy of ~25 meV (~200 cm^{-1}). This means that structural and temporal information can be measured simultaneously.

The reader is reminded that the scattering of neutrons is usually treated as the sum of two parts, known as *coherent* and *incoherent* scattering. To understand why such a separation is performed recall that the strength of the scattering from nuclei of the same element can vary (and generally does vary) with spin and/or isotopic species. Hence when a neutron is scattered by a collection of nuclei the interference between the different scattered waves is normally neither complete nor completely absent. For this reason the *double differential cross section* $[d^2\sigma/d\Omega d\omega]$, which describes the probability that neutrons are scattered into solid angle $d\Omega$ and energy transfer window $d(\hbar\omega)$, is normally separated into two terms. The first term is the coherent part, which contains all of the interference effects such as Bragg scattering and small angle scattering. The second term is the incoherent scattering, which represents the scattering from individual nuclei and is approximately isotropic. For a single element $[d^2\sigma/d\Omega d\omega]$ can be expressed as

$$\frac{d^2\sigma}{d\Omega d\omega} = \frac{1}{4\pi}\frac{k_f}{k_i}[\sigma_{coh}S(Q,\omega) + \sigma_{inc}S_{inc}(Q,\omega)] \qquad (1)$$

where k_i and k_f are the magnitudes of the initial and final neutron wavevectors, σ_{coh} and σ_{inc} are the coherent and incoherent scattering cross sections, and $S(Q,\omega)$ and $S_{inc}(Q,\omega)$

are the corresponding scattering functions which depend only on the momentum transfer $\hbar Q$ (or wave vector transfer Q) and the energy transfer $\hbar\omega$. (Note that in general Q is a vector but since we shall be working with a cubic symmetry powder, which has no preferred orientation, all that need concern us in this experiment is the magnitude of the vector.) The most important incoherent scatterer is hydrogen for which σ_{inc}= 80 barns/atom whereas σ_{coh} is only 1.76 barns/atom (1 barn = 10^{-24}cm^2). Since the incoherent scattering cross section of hydrogen is much larger than those of almost all other nuclei, it is often reasonable (as a first approximation) to neglect the coherent scattering in systems that contain a relatively large fraction of hydrogen atoms. Carbon, on the other hand, is mostly a coherent scatterer with σ_{coh} = 5.55 barns/atom and a negligible incoherent cross section necessitating the use of the 'incoherent approximation' when relating the one-phonon part of incoherent scattering cross section to the generalized vibrational density of states. This is essentially a statement that an integral of the double differential cross section, for a coherent scatterer, over a sufficiently large Q-range is approximately equal to its incoherent counterpart.

Can you explain the usefulness of deuteration, given that σ_{coh}(deuterium) and σ_{inc}(deuterium) are 5.6 barns/atom and 2 barns/atom, respectively?

Elastic neutron scattering is scattering with no change in neutron energy, i.e. with $\hbar\omega = 0$, and *inelastic neutron scattering* is scattering with a change in neutron energy, i.e. with $\hbar\omega \neq 0$. On the other hand, *quasielastic neutron scattering* (QENS) involves the Doppler-like broadening of otherwise elastically scattered neutrons due to reorientational or diffusive motions of atoms in the target material. Thus QENS is a special kind of inelastic neutron scattering. In this experiment we shall use elastic, inelastic and quasielastic neutron scattering to obtain a physical description of the phase change and dynamics of C_{60} at ~260 K, and to gain insights into the origin of the diffuse scattering observed in the powder diffraction data (figure 2).

We shall first describe the sample to be used for the experiment, and the equipment that will be used to bring samples to the desired measurement temperature. The next section gives a brief discussion of the spectrometer as well as matters to be considered in choosing the incident wavelength for this experiment. We then describe the reduction of the data to obtain the scattering function $S(Q,\omega)$, and we follow with some words about the scattering that is expected for the two phases. This then sets the scene for the analysis and discussion of the experimentally measured scattering function.

II. The sample

Prior to the experiment ~15 grams of the C_{60} sample will have been loaded into a tall (10cm, diameter 1.3 cm) aluminum cell with some helium exchange gas and press sealed with indium wire. At the start of the experiment we shall mount the sample in a closed cycle helium refrigerator, and we shall decide on an initial temperature set point and wavelength. Through the night we shall collect data at the initial temperature and wavelength, and at other temperatures and/or wavelengths.

Why do we typically use aluminum for sample containers and cryostat windows?

Apart from indium, what materials might be used to seal sample containers?

To reduce the data we will need a detector normalization file obtained using a sample of vanadium metal, plus a run with the beam closed (a type of background). These runs will have been performed before the start of the summer school since there will not be time to complete them during the school.

Why do we use vanadium to normalize the data from different detectors? Hint: σ_{coh}= 0.02 barns/atom, σ_{inc}= 5.19 barns/atom.

III. The spectrometer

We shall be performing this experiment using the Disk Chopper Spectrometer (DCS), which is a so-called "direct geometry" (fixed incident energy) time-of-flight spectrometer. In this type of instrument (figure 4) bursts of monochromatic neutrons strike the sample at equally spaced times. The energies of the scattered neutrons are determined from their arrival times at the detectors, since we know when the pulses were created as well as the distances D_{PS} from the pulsing device to the sample and D_{SD} from the sample to the detectors. There are two ways to produce a monochromatic pulsed beam at a steady state neutron source. One method is to use a single crystal to monochromate the white beam and a mechanical "chopper" to pulse it; the other method is to use multiple choppers, such as the seven (!) choppers of the DCS.

A monochromatic pulsed beam of neutrons can in principle be created using two choppers. How does that work? Can you think why more than two choppers might be needed and/or desirable?

Given the initial and final energies of the neutrons, E_i and E_f, the energy transfer $\hbar\omega = E_i - E_f$ is trivially obtained. Knowing the scattering angle 2θ we can also calculate the magnitude of the momentum transfer to the sample, $\hbar Q$:

$$(\hbar Q)^2 = 2m_n\left[E_i + E_f - 2\sqrt{E_i E_f}\cos 2\theta\right] \qquad (2)$$

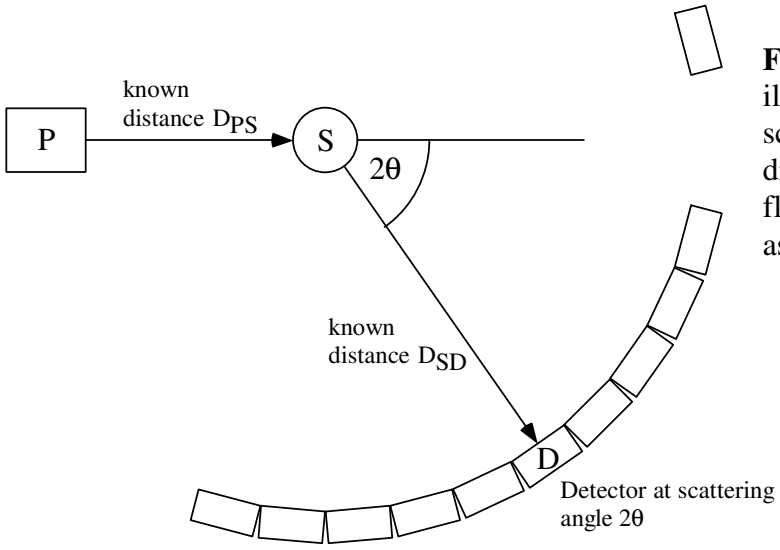

Figure 4. A schematic illustration of the scattering geometry for a direct geometry time-of-flight spectrometer such as the DCS.

where m_n is the mass of the neutron. (This follows from the definition $\vec{Q} = \vec{k_i} - \vec{k_f}$ and the relationship between the magnitude of a neutron's wave vector, k, and its energy E: $E = \hbar^2 k^2 / 2m_n$.)

The data acquisition system separately accumulates neutron counts for each of the 913 DCS detectors. Furthermore the time between pulses, T, is normally divided into 1000 time channels of equal width $\Delta t = 0.001T$ and each neutron event in a given detector is stored in one of these time channels according to its time of arrival at the detector. Thus the data acquisition system generates a two-dimensional array of counts I(i,j) as a function of detector index i and time channel index j. This array is accumulated in a "histogramming memory" which is resident in the data acquisition computer and reflected to the instrument computer. At the end of each run cycle the array is saved, along with other pertinent information, to the hard disk of the instrument computer.

At the DCS we shall first mount the sample on the sample table, taking care to position it correctly with respect to the incoming beam; to confirm the positioning of the sample we may use a Polaroid camera or a TV camera system adapted for use with neutrons. We shall bring the sample to its measurement temperature having connected the temperature controller to the instrument computer so that we can record the sample's temperature throughout the experiment.

An incident wavelength will then be selected, together with other instrument parameters such as the "master speed" of the choppers. The choice of wavelength is critical and several factors must be considered. These include intensity at the sample (which peaks, remaining roughly constant, between ~2.5 and ~4.5 Å, see Appendix A), the width of the elastic energy resolution function (which roughly varies as $1/\lambda^3$), the available Q range (which varies as $1/\lambda$), and concerns about "frame overlap" problems. A related consideration is the available range in sample energy gain (neutron energy loss).

> What is the maximum theoretical sample energy gain that can be measured when the incident energy is E_i, and how long would it take to measure the intensity of neutrons scattered with this change in energy?

Once the sample is at temperature, with the choppers phased, we will be ready to define the measurements to be performed through the night. We shall define a "sequence" consisting of several "runs" plus at least one change of sample temperature and probably wavelength. We shall also define the individual runs. Each run is divided into a set of "cycles". At the end of each cycle the temperature is recorded and the data are backed up to the disk. Having defined the runs we shall start the overnight sequence of measurements. Next day we shall stop the measurements and start into the data reduction.

In the experimental runs we shall collect intensity histograms I(i,j) for C_{60} at a couple of temperatures. Using previously acquired intensity histograms for a vanadium sample and for a "dark count" run with the beam shutter closed, we shall reduce the data to obtain the double differential scattering cross section $[d^2\sigma/d\Omega d\omega]$, the scattering function $S(Q,\omega)$, and various cuts in both Q and ω, and the generalized phonon densities of states g(ω).

IV. Data reduction

In this section we shall simply indicate some of the more important steps in the data reduction process. We shall go into greater detail in our discussions at the time that the data reduction takes place.

The measured scattering from the C_{60} sample has components from the intrinsic scattering from the sample and background intensity. Before doing any data analysis we need to subtract a time independent background from each of the runs.

> Where does the time independent background come from?

Neglecting effects such as self-shielding and multiple scattering the scattering in detector i and time channel j may be related to the corresponding double differential cross section $[d^2\sigma/d\Omega dt]_{ij}$ (note that this is per unit time, not energy) in the following fashion:

$$I(i,j) = \frac{I_{BM}}{\eta_{BM}} \cdot \left[\frac{d^2\sigma}{d\Omega dt}\right]_{ij} \Delta\Omega\Delta t \cdot N_m \cdot \eta_{ij} \qquad (3)$$

where $\Delta\Omega$, the solid angle subtended by detector i, and Δt, the width of time channel j, are (for these measurements) presumed to be independent of i and j respectively, N_m is the number of sample molecules in the beam, η_{ij} is the efficiency of detector i for neutrons detected in time channel j, and I_{BM} and η_{BM} are respectively the counts and the efficiency of the beam monitor (situated upstream of the sample).

Since we are not trying to extract an absolute cross section we can neglect the multiplicative constants in the above equation, but we should not ignore the detector efficiency function η_{ij}. Since all of the detectors are to first order identical it is not unreasonable to treat η_{ij} as the product of two terms, a function η_{i0} which represents the efficiency of detector i for elastically scattered neutrons and a detector-independent function f_j that describes the energy dependence of the efficiency of the detectors. The correction for differences in detector response, i.e. the determination of η_{i0}, is performed using the results of a measurement with a vanadium sample.

The correction of the data for the energy dependence of the efficiency is achieved by calculation, knowing the various factors that affect the probability that a neutron is absorbed within a detector.

What are these factors?

To improve statistics, in some instances, we may define several detector groups, each of which includes detectors within a specified range of angles. The differential cross section $[d^2\sigma/d\Omega dt]$ for all detectors in a group will be summed and divided by the number of detectors in the group. Having obtained a quantity proportional to $[d^2\sigma/d\Omega dt]$ we must now compute $[d^2\sigma/d\Omega d\omega]$ and finally $S(Q,\omega)$. Since a neutron's energy E is related to its time-of-flight t over a fixed distance as $E \propto t^{-2}$, it follows that $dE \propto t^{-3}dt$. Hence

$$\frac{d^2\sigma}{d\Omega d\omega} \propto \frac{d^2\sigma}{d\Omega dE_f} = \left[\frac{d^2\sigma}{d\Omega dt}\right]\left(\frac{dt}{dE_f}\right) \propto \left[\frac{d^2\sigma}{d\Omega dt}\right] t^3 \qquad (4)$$

To obtain $S(Q,\omega)$ we simply divide by k_f (see eq. 1). Equivalently we multiply by another factor of t.

If a system in thermodynamic equilibrium can exist in a number of thermodynamic states and we consider two such states separated by an energy difference $\hbar\omega$, the probability that the system is in the lower energy state is greater by a factor $\exp(\hbar\omega/kT)$ than the probability that it is in the higher energy state. From this it can be shown that for systems in thermodynamic equilibrium the scattering function $S(Q,\omega)$ satisfies the so-called "detailed balance" relationship: $S(-Q,-\omega) = \exp(-\hbar\omega/kT)S(Q,\omega)$. Since we shall be fitting the data to a theoretical form that is symmetric in $\hbar\omega$ we shall first "symmetrize" the experimental $S(Q,\omega)$ by multiplying it by $\exp(-\hbar\omega/2kT)$.

Is symmetrization of $S(Q,\omega)$ likely to be a larger effect at low or high temperatures?

Having reduced the experimental data to a symmetrized scattering function it is time to relate the results to theory.

V. Theory

The reorientational character of diffusive motion in the high temperature phase of C_{60} is reflected in the Q dependence of the quasielastic scattering. A model in which the rotations of adjacent molecules are uncorrelated and individual molecules undergo rotational diffusion about their fixed centers follows. In this section we shall revert to using the subscript "coh" and we shall treat Q as a vector.

In a classical treatment the angular motion of each molecule satisfies the differential equation (Fick's Law/Brownian diffusion):

$$D_R \nabla_\Omega^2 p(\Omega,\Omega_0,t) = \frac{\partial}{\partial t} p(\Omega,\Omega_0,t), \tag{5}$$

where D_R is the rotational diffusion constant, ∇_Ω^2 is the Laplacian operator in the space of Euler angles Ω, and $p(\Omega,\Omega_0,t)$ is the probability that a molecule has orientation Ω at the time *t*, having had the orientation Ω_0 at time 0. This model implies the molecule tumbles through a continuum of orientational angles rather than jumping between discrete orientations. A powder average can then be expressed as a sum of Lorentzians

$$S_{coh}^{rot}(\vec{Q},\omega) = \sum_{\ell=1}^{\infty} a_\ell (2\ell+1) j_\ell^2(\vec{Q}R) \frac{1}{\pi}\left[\frac{\tau_l}{1+\omega^2\tau_l^2}\right] \tag{6}$$

where

$$\tau_\ell = \frac{1}{\ell(\ell+1)D_R} \tag{7}$$

j_ℓ is a spherical Bessel function, and R is the radius of the C_{60} molecule. The coefficients a_ℓ are in this case given by

$$a_\ell = \sum_{n,n'=1}^{60} P_\ell(\cos\theta_{nn'}) \tag{8}$$

where P_ℓ is a Legendre polynomial and $\theta_{nn'}$ is the angle between the position vectors joining the molecular center to atoms *n* and *n′* within a single molecule. The high symmetry of the C_{60} molecule means that all odd-ℓ and many even-ℓ terms are identically zero. The only terms that significantly contribute to the scattering in the *Q*-range of these experiments are those with ℓ=6, 10, 12, 16, 18 and 20 for which the sum over the P_ℓ takes the values 6.3, 224, 31, 123, 496 and 90, respectively.

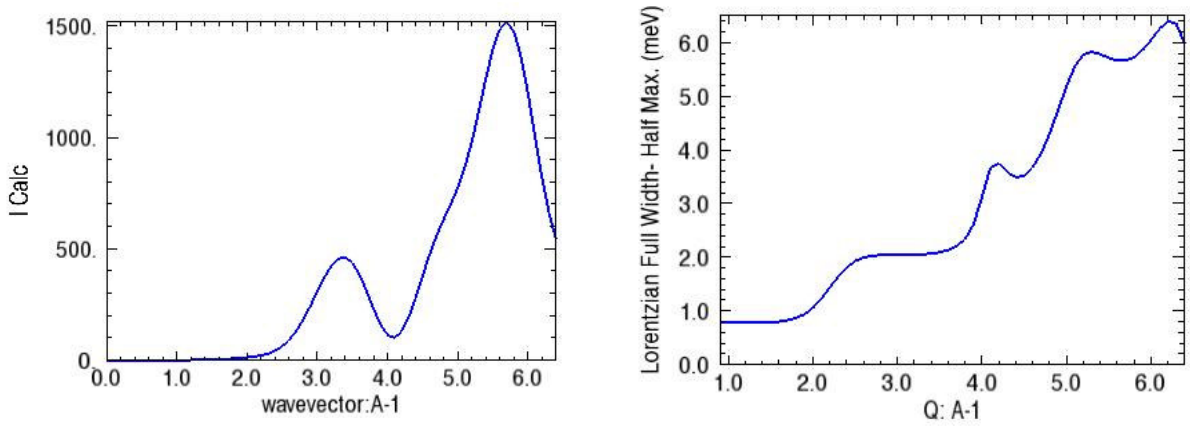

Figure 5. The expected quasielastic intensity and equivalent single Lorentzian width, as a function of momentum transfer, for a rotationally diffusing C_{60} molecule.

Even though the quasielastic scattering is a sum of Lorentzians, the original literature on this subject approximates this as a single Lorentzian (FWHM= $2/\tau_\ell$) and this was sufficient for the quality of those data. The integrated intensity and equivalent single Lorentzian width, according to the rotational diffusion model, eqn. 6, are shown in fig. 5. It may be that you will need to include more than one Lorentzian when fitting your data, plus a Gaussian to account for any elastic Bragg scattering contributions. Writing $D_R = 1/6\tau_{NMR}$ the value of D_R can be compared with NMR correlation times τ_{NMR}: 12 ps at 300 K and 9 ps at 283 K. Activation energies derived from NMR range from 42(9) meV to 60(5) meV.

Can you use this information to define the origins of the diffuse scattering observed in the powder diffraction data?

On cooling through the 260 K transition the quasielastic scattering is replaced by inelastic features and the diffuse scattering is different. Apart from an angular Debye-Waller factor, and an extra thermally averaged correlation function, the energy integral over the librational peaks follows eqn.6 with an extra $\ell(\ell+1)$ factor favoring the higher ℓ-terms. The librational peaks soften and broaden on heating. The intensity variation of these peaks follows that expected for a simple harmonic oscillator

$$\frac{1}{\omega_0(T)}\frac{e^{\hbar\omega_0(T)/2kT}}{e^{\hbar\omega_0(T)/2kT}-1} \tag{9}$$

of frequency $\omega_0$at temperature T. This is in contrast to the librational frequency that softens much more than expected.

The librations themselves are a probe of the curvature of the rotational potential near the potential minimum. For example, a uniaxial rotational potential $V(\theta)$, can be expanded in a Fourier series as

$$V(\theta) = -\sum_{n=0}^{\infty} \frac{1}{2} V_n [1 - \cos(n\theta)] \tag{10}$$

Within the harmonic approximation, the energy of the librational excitation is given by

$$\hbar\omega = \hbar \left[\frac{1}{I} \frac{\partial^2 V(\theta)}{\partial \theta^2} \bigg|_{\theta=0} \right]^{1/2} \tag{11}$$

i.e.

$$\hbar\omega = \hbar \left[B \sum_{n=1}^{\infty} n^2 V_n \right]^{1/2} \tag{12}$$

where I is the moment of inertia and $B = \hbar^2/2I$ is the rotational constant. For C_{60}, $I \simeq 1 \times 10^{-43}$ kg m^2 and $B \simeq 0.364\,\mu$eV.

With C_{60} we cannot really say that we have a single molecular axis since there are several local minima in the orientational potential, but we may assume that the index of the dominant term can be expressed by $n = 2\pi/\theta_{hop}$, where θ_{hop} is an angle between adjacent minima in the orientational potential. Then

$$\hbar\omega = (2\pi/\theta_{hop})\sqrt{BV_A} \tag{13}$$

where V_A, the activation energy for rotational jumps between adjacent minima, can be determined from a number of techniques and is on the order of 220-290 meV. One consistent view of the reorientation mechanism involves ~42^o hops about 2-fold axes that are normal to the body diagonals. This model is almost isotropic.

VI. Data analysis

We will take a few detours on the route to obtaining a symmetrized form of the experimental scattering function, $S(Q,\omega)$. We will sum data to obtain a view of the powder diffraction patterns at various temperatures and we will also sum to obtain a generalized vibrational densities of states that we will then compare to data taken on the FANS spectrometer and briefly discuss the significance of what is observed.

The next step is to fit the $S(Q,\omega)$ data above 260 K to a model. We suggest that you try fitting each Q group to the isotropic rotational diffusion model described in the previous section (i.e. an elastic delta function and a broader Lorentzian). In an actual experiment the scattering function is broadened with the instrumental resolution function so the model function must be numerically convoluted with the instrumental resolution function. Having fitted the experimental data to the model, the next step is to make plots of the Lorentzian line parameters as functions of Q.

(1) How well does the single Lorentzian fit?
(2) Do the Lorentzian parameters behave similarly to fig. 5?
(3) Can you extract an activation energy and rotational timescale?
(4) Can you explain how the diffraction data and the QENS data relate to one

Perform a similar analysis for the lower temperature data; fitting a central Gaussian and two librational Lorentzian peaks. Plot the temperature dependence of the Lorentzian parameters, and fit a functional form (eqn. 9.) to the extracted intensities. Use eqn.12 to extract an activation energy.

VII. Concluding remarks

In section V we discussed a scattering function that corresponds to very simple model of coherent rotational diffusive motion. The situation is more complicated when a system displays more than one type of diffusive motion, or rotational axes. If the various motions are uncoupled, the intermediate scattering function is a product of the individual intermediate scattering functions so that the scattering function is a convolution of the scattering functions for the individual motions. The situation simplifies considerably if additional motions occur on very different time scales. Motions that are much slower than the time scale represented by the instrumental resolution show up as elastic scattering. On the other hand motions that are much faster give rise to an essentially flat background. Different instruments, with different dynamical windows and different resolution capabilities, are needed to observe such motions. For example motions that are too slow to see using the DCS may well show up if the sample is put on the backscattering spectrometer. Conversely motions that are fast by DCS standards can usefully be studied using the FANS facility.

VIII. General references

- J.R.D. Copley *et. al*, "Neutron Scattering Studies of C_{60} and its Compounds", J. Phys. Chem. Solids. **53**, 11, 1353 (1992)
- G.E. Bacon, "*Neutron Diffraction*", Clarendon Press, Oxford (1975).
- M. Bée, "*Quasielastic Neutron Scattering*", Adam Hilger, Bristol (1988)
- R. Hempelmann, "*Quasielastic Neutron Scattering and Solid State Diffusion*", Clarendon Press, Oxford (2000).
- S.W. Lovesey, "*Theory of Thermal Neutron Scattering from Condensed Matter*", Clarendon Press, Oxford (1987).
- G.L. Squires, "*Introduction to the Theory of Thermal Neutron Scattering*", Cambridge University Press (1978), republished by Dover (1996).

Appendix A. Instrument Characteristics for the Disk Chopper Spectrometer

(http://www.ncnr.nist.gov/instruments/dcs)

The white beam from the cold neutron source is cleaned of high energy neutron and gamma ray contamination using an "optical filter". This is basically a bent guide which ensures that there is no line of sight from the source to points beyond the local shutter. A cooled graphite filter removes short wavelength (~0.5 Å) neutrons that remain in the beam, permitting measurements at wavelengths down to roughly 1.5 Å.

A clean, pulsed, monochromatic neutron beam is produced using seven disk choppers. Chopper speeds may be varied from 1200 to 20000 rpm. The pulsing and monochromating choppers have three slots of different widths. In principle this permits three choices of intensity and resolution at a given wavelength and master chopper speed.

The measured intensity at the sample is reproduced below. Red and blue points (upper and lower plots) correspond to measurements using different chopper slot widths.

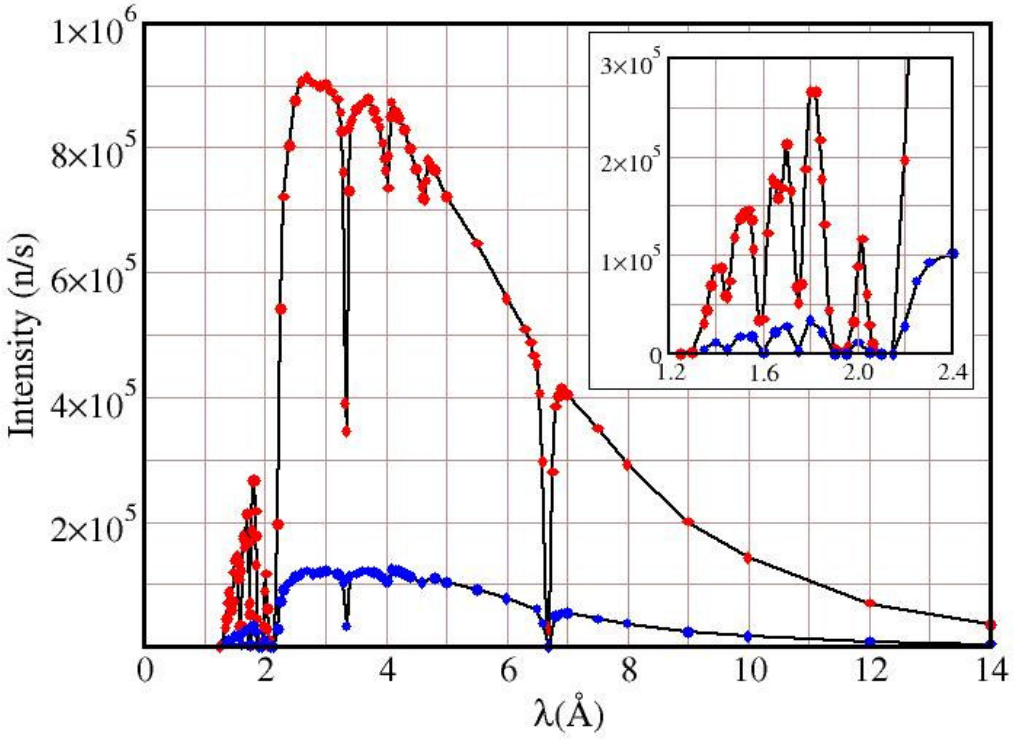

Why are there dips in the measured flux at wavelengths near 3.335 and 6.67 Å? What's going on around 2 Å?

The resolution of the instrument is approximately triangular and essentially independent of beam height (10 cm) but depends on the width of the beam. Hence samples should ideally be tall and thin rather than short and fat.

The measured elastic energy resolution, for the same choices of chopper slot width as in the intensity plot above, is shown in the figure below. Lines represent fits to the measurements.

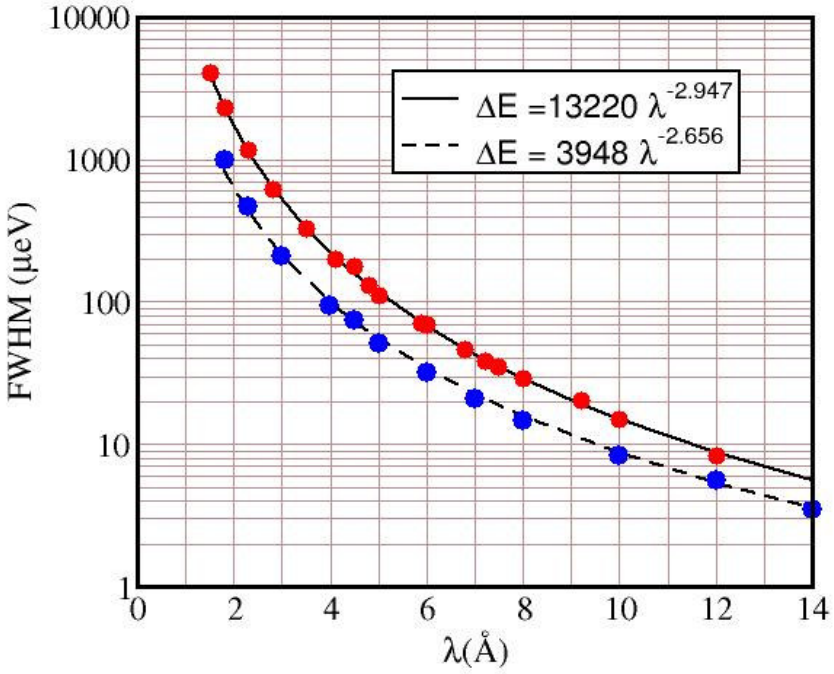

An oscillating radial collimator, inside radius 200 mm, outside radius 300 mm, blade separation 2°, is used to reduce the scattering from sample environment structures.

Can you explain how the radial collimator works, and why it is oscillated?

There are 913 six atmosphere ^{3}He detectors covering an essentially continuous solid angle of ~0.65 steradians and arranged in three banks:

- Middle bank detector scattering angles range from -30° to -5° and from +5° to +140°
- Upper and lower bank angles range from -30° to -10° and from +10° to +140°

The flight distance from sample to detectors is 4010 mm. The flight chamber is purged with argon.

Why is the flight chamber purged with argon?

Appendix B. Possible Experiments on the Disk Chopper Spectrometer

Phenomena that can be investigated include:

- Translational and rotational diffusion processes, where scattering experiments provide information about time scales, length scales and geometrical constraints; the ability to access a wide range of wave vector transfers, with good energy resolution, is key to the success of such investigations
- Low energy vibrational and magnetic excitations and densities of states
- Tunneling phenomena
- Low Q powder diffraction

Research areas include:

- **Chemistry ---** e.g. clathrates, molecular crystals, fullerenes
- **Polymers ---** bound polymers, glass phenomenon, confinement effects
- **Biological systems ---** protein folding, protein preservation, water dynamics in membranes
- **Physics ---** adsorbate dynamics in mesoporous systems (zeolites and clays) and in confined geometries, metal-hydrogen systems, glasses, magnetic systems
- **Materials ---** negative thermal expansion materials, low conductivity materials, hydration of cement, carbon nanotubes, proton conductors, metal hydrides

Appendix C. Some useful properties and relationships

Neutron properties

Mass:	1.660×10^{-24} g
Electric charge:	0
Spin:	½
Magnetic moment:	-1.913 nuclear magnetons

Exact relationships

$$\lambda = \frac{h}{mv} \qquad E = \frac{1}{2}mv^2 \qquad k = \frac{2\pi}{\lambda}$$

Approximate relationships

$$E[\text{meV}] = \frac{81.8}{(\lambda[\text{Å}])^2}; \quad v[\text{mm}/\mu\text{s}] = \frac{3.956}{\lambda[\text{Å}]}; \quad E[\text{meV}] = 2.07(k[\text{Å}^{-1}])^2; \quad 1\ \text{meV}=8.1\ \text{cm}^{-1}$$

Appendix D. Spin Incoherence

The strength of the scattering of a neutron by a nucleus, i.e. the neutron scattering length, depends on the spin of the compound nucleus. For an isotope with nuclear spin I the combined "nucleus + neutron" spin, I′, has two possible values, $I^+ = I+1/2$ and $I^- = I-1/2$, with which we associate two possible scattering lengths b^+ and b^-. Each of the possible values of the combined spin has $2I'+1$ possible spin states, i.e. $2(I+1/2)+1 = 2I+2$ and $2(I-1/2)+1 = 2I$ states respectively, for a total of $4I+2$ spin states.

If the neutron and nuclear spins are randomly orientated, all states are equally probable, and the probabilities of the combined + and - spin states are $p^+ = (I+1)/(2I+1)$ and $p^-=I/(2I+1)$ respectively.

The mean scattering length, $\langle b \rangle$, and the mean of the scattering length squared, $\langle b^2 \rangle$,

$$\langle b \rangle = p^+b^+ + p^-b^- \quad \text{and} \quad \langle b^2 \rangle = p^+(b^+)^2 + p^- (b^-)^2$$

are used to calculate the coherent and incoherent bound cross sections. These cross sections are defined as follows:

$$\sigma_{coh} = 4\pi\langle b\rangle^2 \quad \text{and} \quad \sigma_{inc} = 4\pi\left(\langle b^2\rangle - \langle b\rangle^2\right).$$

Working through the numbers for hydrogen and deuterium is instructive. The relevant scattering lengths for hydrogen are $b^+ = 1.086\times10^{-12}$ cm and $b^- = -4.751\times10^{-12}$ cm, whereas the values for deuterium are $b^+ = 0.951\times10^{-12}$ cm and $b^- = 0.095\times10^{-12}$ cm.